Chapter 2: Photoswitching of DNA Hybridization using a Molecular Motor

Reversible control over the functionality of biological systems via external triggers may be used in future medicine to reduce the need for invasive procedures. Additionally, externally regulated biomacromolecules are now considered as particularly attractive tools in nanoscience and the design of smart materials, due to their highly programmable nature and complex functionality. Incorporation of photoswitches into biomolecules, such as peptides, antibiotics and nucleic acids, has generated exciting results in the past few years. Molecular motors offer the potential for new and more precise methods of photoregulation, due to their four-state switching cycle, unidirectionality of rotation, and helicity inversion during the rotational steps. Aided by computational studies, a photoswitchable DNA hairpin is designed and synthesized, in which a molecular motor serves as the bridgehead unit. After determining that motor function was not affected by the rigid arms of the linker, solid phase synthesis was employed to incorporate the motor into an 8 base pair self-complementary DNA strand. With the photoswitchable bridgehead in place, hairpin formation was unimpaired, while the motor part of this advanced biohybrid system retains excellent photochemical properties. Rotation of the motor generates large changes in structure, and as a consequence the duplex stability of the oligonucleotide could be regulated by UV light irradiation. Additionally, Molecular Dynamics computations were employed to rationalize the observed behaviour of the motor-DNA hybrid. The results presented in this chapter establish motors as powerful multistate switches for application in biological environments.

Part of this chapter was published as: T. M. Neubauer, T. van Leeuwen, D. Zhao, A. S. Lubbe, J. C. M. Kistemaker, B. L. Feringa, *Org. Lett.* **2014**, *16*, 4220–4223.

Part of this chapter is currently submitted for publication.

2.1 Introduction

DNA carries the genetic information of all known organisms. In the more than 60 years since Watson, Crick and Franklin unravelled the double helix,[1] immense advances have been made in our understanding of DNA structure and function. Moreover, the programmable nature of DNA has led to its use in nanotechnology,[2] genetic engineering,[3] information storage[4] and a range of other applications. In the ongoing search to understand and control the key processes of life, the ability to modulate DNA structure and function is highly desired. Various triggers, such as pH change,[5] small molecules,[6] short primers,[7] biological signals,[8] heat[9] and light,[10–12] have been applied to achieve this goal. Of these, the use of light has distinct advantages over the other triggers. Light is non-invasive to living tissue, and a high level of spatial and temporal control over its application is possible.[10] Therefore, light-responsive molecular switches (photoswitches) are considered particularly attractive for reversible control over poly- and oligonucleotide structure and function.[11,12]

In photoregulation of oligonucleotides, extensive use is made of hairpin structures, which comprise short loops of hybridized, self-complementary DNA or RNA. They can form naturally and are frequently found in RNA secondary structure, where, among a variety of functions, they guide folding, protect mRNA from degradation and act as recognition sites or substrates for enzymatic reactions.[13,14] Hairpins are short oligonucleotides and are therefore relatively easy to synthesize, while their self-hybridization is a small-scale model for double stranded DNA hybridization.[15] Typically in preparing photoresponsive hairpins, the bridging nucleotides of the loop are replaced by a molecular photoswitch. The photoswitch is usually incorporated into the phosphate backbone of the oligonucleotide. In one state, the switch stabilizes the double stranded helix structure. Irradiation causes a conformational change in the structure of the switch, which leads to destabilization of the helix and a lower melting temperature (T_m). Ideally, in a certain temperature range, the oligonucleotide can be fully switched between double and single stranded structures. As a result, in that specific temperature range the structure can exist as a 'closed' double stranded form, or as an 'open' single stranded form, which may engage in interactions with other biomolecules.

Backbone incorporation of photoswitches was pioneered by Letsinger and Wu,[16,17] using stilbenes as photoactive bridging units; subsequently this method was expanded with the use of azobenzenes by Yamana and co-workers.[18] Both *trans*-stilbene and *trans*-azobenzene stabilize the hairpins through π-π interactions with neighbouring nucleobases. Upon switching to the nonplanar *cis* isomer, the extra stabilization is lost, leading to a lower T_m. This effect was enhanced by Sugimoto and co-workers, by a precise engineering of the azobenzene backbone linker length (**2.2**, see Figure 2.2).[19] In their design, the *cis* isomer of the photoswitchable backbone linker is too short to function as a bridgehead for the hairpin. Therefore, the hairpin is distorted upon *trans* to *cis* isomerization, leading to additional destabilization and lowering of the T_m. The difference in T_m

(ΔT_m) between the two isomers was found to be 20 °C for a 5 base pair (bp) hairpin (5'-AAAAG-**2.2**-CTTTT-3'). The ΔT_m is highly dependent on hairpin length and sequence, and drops to 17.3 °C if the base pair adjacent to the bridgehead is changed to A-T (5'-AAAAA-**2.2**-TTTTT-3'), and to 13.9 °C for a 6 bp hairpin ((5'-AAAAAA-**2.2**-TTTTTT-3')).[20] Regardless, by the use of an ingenious linker design, Sugimoto and co-workers were able to achieve an unusually high ΔT_m by the incorporation of only a single molecular photoswitch.[19]

Overcrowded alkene-based rotary molecular motors offer novel opportunities in the field of photoregulation of biologically active molecules due to their unique dynamic properties. The first of this type of responsive molecules was reported in 1999 and was of particular interest because it exhibited repetitive, photochemically driven unidirectional rotation around a carbon-carbon double bond.[21] In recent years, however, molecular motors have found a vast range of applications as multistate switches. The rotary cycle of an overcrowded-alkene based molecular motor consists of four steps and it therefore features four different isomers. Scheme 2.1 shows the complete rotary cycle of a first generation molecular motor **2.1**.[22] Starting from the stable *trans* isomer, irradiation with λ = 312 nm light leads to photochemical *trans-cis* isomerization. The resulting unstable *cis* isomer suffers a significant steric strain, because the stereogenic methyl substituents are forced in an unfavourable pseudo-equatorial conformation. While the photoisomerization is reversible, the equilibrium usually lies to the right. The steric strain of the unstable *cis* isomer can be released by a thermal helix inversion (THI). In the resulting stable *cis* isomer the methyl substituents are returned to an energetically favourable pseudo-axial configuration. The thermal helix inversion is irreversible and proceeds in quantitative yield. The half-life of the unstable *cis* isomer in five membered ring-xylene based first generation molecular motors is typically rather long (for motor **2.1**, $t_{1/2}$ > 1.5 d at rt in hexane). For the second half of the rotary cycle, the stable *cis* isomer is irradiated with λ = 312 nm light to generate the unstable *trans* isomer. Subsequently, THI leads to the stable *trans* isomer and a 360° rotational cycle is completed. The half-life of the unstable *trans* isomer is typically much shorter (for motor **2.1**, $t_{1/2}$ = 1.2 s at rt in hexane) than the half-life of the unstable *cis* isomer.

The large geometrical change upon *cis-trans* isomerization in rotary molecular motors, accompanied by the structural rigidity, are particularly suited to induce a significant structural change in a DNA hairpin upon irradiation. Moreover, the four-state switching cycle and the change in helicity of the motor in each rotary step offer potential for new functionalities and high degree of photoregulation. With this in mind, the possibility of using a molecular motor to reversibly control the hybridization of a DNA hairpin was evaluated.

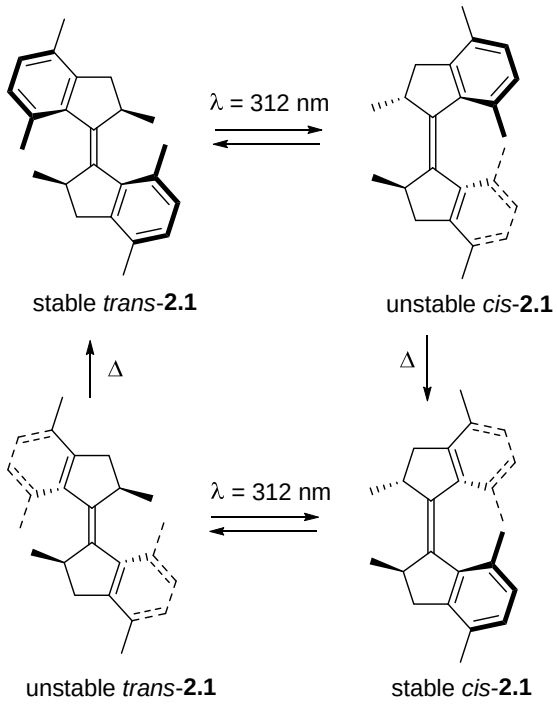

Scheme 2.1: Photochemical and thermal isomerization processes during 360° unidirectional rotary cycle of first generation artificial molecular motor **2.1**.

Figure 2.1 depicts a schematic overview of the proposed photoswitchable hairpin. Inspired by the successful design of Sugimoto and co-workers,[19] it was envisioned that one of the isomers (in this case stable *cis*) can be accommodated as a loop element of the hairpin. An even larger geometrical effect may be induced by using an expanding linker instead of a contracting one.

Upon *cis-trans* isomerization, the motor-bridgehead expands considerably, leading to a destabilization of the hairpin and a corresponding decrease in melting temperature. As a result, at a temperature range around the recorded T_m's, the equilibrium between the DNA double helical hairpin structure and the single stranded form can be shifted towards the latter, by a photoinduced isomerization of the *cis* form (which forms relatively stable hairpins) to the more destabilized *trans* form. Here, the stable isomers of the motor were synthesized separately to determine the T_m for each isomer, after which UV-vis spectroscopy was used to examine the switching behaviour of the hybrids.

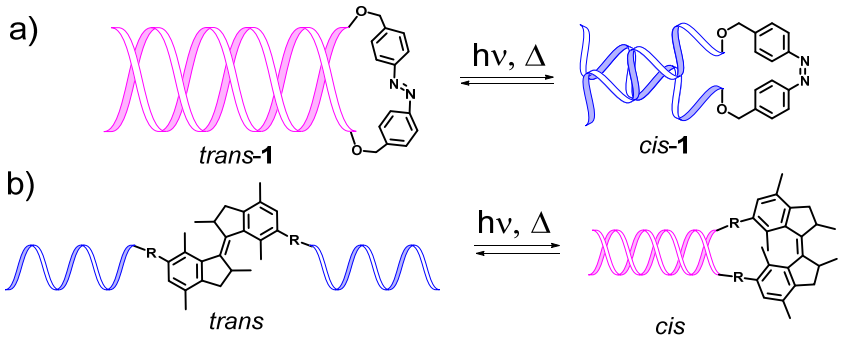

Figure 2.1: Schematic overview of the photoswitchable DNA hairpins. (a) Design by Sugimoto and co-workers based on photoswitchable linker **2.2**. (b) Concept for linker based on first generation molecular motors.

2.2 Computational-aided molecular design of the linker

Before starting the synthesis of the target motor-hairpin hybrid, calculations were performed to ensure that the design would be optimal for the envisioned application. By analogy to the azobenzene **2.2** (Figure 2.2) reported by Sugimoto and co-workers,[19] a double primary alcohol functionalized motor was designed, which could be incorporated in the DNA strand through standard solid phase DNA synthesis (SPS). The ideal design should have an O-O distance of 13.3 Å, which is the optimal bridgehead length, in the stable *cis* isomer. The O-O distance should be as large as possible in the *trans* isomer. Rigid side chains are necessary to enforce sufficient distortion of the hairpin upon photochemical switching. A first generation motor was preferred, because they are symmetrical, have limited conformational flexibility and therefore maximize geometrical change.

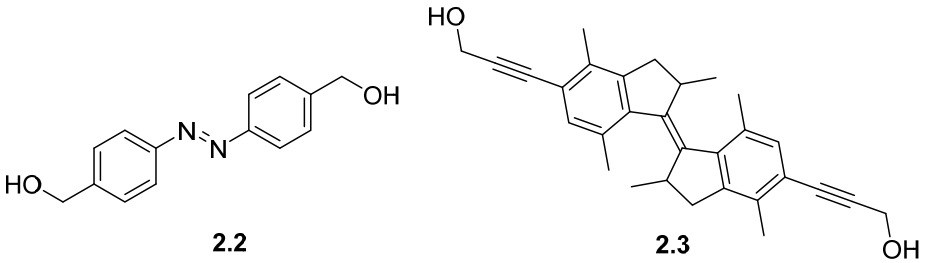

2.2 **2.3**

Figure 2.2: Structures of azobenzene linker **2.2** and motor linker *trans*-**2.3**.[19]

Two designs were investigated computationally using Density Functional Theory (DFT). For a detailed description of these calculations, see reference 23. Of the two designs, motor **2.3** (Figure 2.2) was selected as the most ideal candidate. Based on the computations, it was concluded that switching from *cis* to *trans* in a DNA hairpin containing motor **2.3** as a bridgehead unit will lead to a significant destabilization of the hairpin.

2.3 Synthesis of the molecular motor-based linker

The synthesis of *trans*-motor **2.3** is depicted in Scheme 2.2. The preparation of the *trans* isomer is described, but the synthetic route towards the *cis* isomer is identical. The synthesis was started by monolithiation of 2,5-dibromo-*para*-xylene, followed by quenching with methacrolein leading to formation of functionalized xylene **2.4** in near quantitative yield. The secondary alcohol substituent was subsequently oxidized using MnO_2. The resulting α,β unsaturated ketone **2.5** was subjected to a Nazarov cyclization in H_2SO_4 (neat), leading to formation of ketone **2.6** in 83% yield over three steps. Motor **2.7** was generated under McMurry conditions, and obtained in 63% yield as a 1/1.2 mixture of *cis* and *trans* isomers. Notably, isomer separation could be performed at this stage in the synthesis by crystal picking. While *cis*-**2.7** crystallizes in a cubic shape, *trans*-**2.7** forms needles.

Asymmetric synthesis of motor **2.7** could be performed on preparative scale.[24] However, for the sake of synthetic simplicity the investigation was commenced using the racemic starting material. The synthesis of both *cis* and *trans* isomers was followed independently. Immediate coupling of **2.7** to the acetylene moieties was unsuccessful. Therefore, the bromine substituents were converted to iodine in a Finkelstein-type reaction. As this reaction was performed at 130 °C, it caused partial thermal isomerization of *trans*-**2.8** to *cis*-**2.8**. After several recrystallization cycles, >95% *trans*-**2.8** could be obtained and the synthesis was continued using *trans*-**2.8** in the presence of a small amount of *cis*-**2.8**. The coupling to the acetylene unit was initially attempted using propargyl alcohol, however, with poor results. The yield was much improved by using propargyl acetate for the Sonogashira coupling. Protected motor **2.9** was obtained in 94% yield which could be converted into target motor **2.3** by a base-mediated deprotection in 87% yield.*

For incorporation in DNA using SPS, motor **2.3** had to be converted in the corresponding phosphoramidite building block **2.11** in two steps (Scheme 2.2). First, one of the primary alcohols of motor **2.3** was protected using one equivalent of dimethoxytrityl (DMT) chloride. From this reaction, a 1:2:1 statistical mixture of starting material **2.3**, monoprotected product **7** and diprotected motor was obtained, which could easily be separated by column chromatography. The resulting monoprotected motor **2.10** was relatively unstable and therefore had to be immediately converted into phosphoramidite motor **2.11**, through a coupling with 2-cyanoethyl-*N*, *N*-diisopropylchlorophosphoramidite. This building block was also highly unstable and was therefore purified by quickly flushing over a SiO_2 column, dissolved in dichloromethane under an argon atmosphere and immediately used in SPS. ^1H and ^{31}P NMR analysis showed that *trans*-**2.11** contained only 20% product. The main impurity ap-

* When the synthesis was first performed, isomer separation proceeded at this stage of the synthesis. *Cis*-**2.3** could be separated from an isomer mixture *via* recrystallization.

peared to be a dimer (structure not shown) resulting from a reaction of starting material **2.10** and product **2.11**, in which the cyanoethyl moiety was replaced by a second motor molecule. As it was established that the hairpin synthesis was not compromised, and to prevent losses by oxidation, a second chromatography was not performed and this mixture was subjected to SPS. In a similar synthesis for the *cis* isomer of motor-based phosphoramidite **2.11**, this final step was highly effective, and *cis*-**2.11** was obtained pure after chromatography.

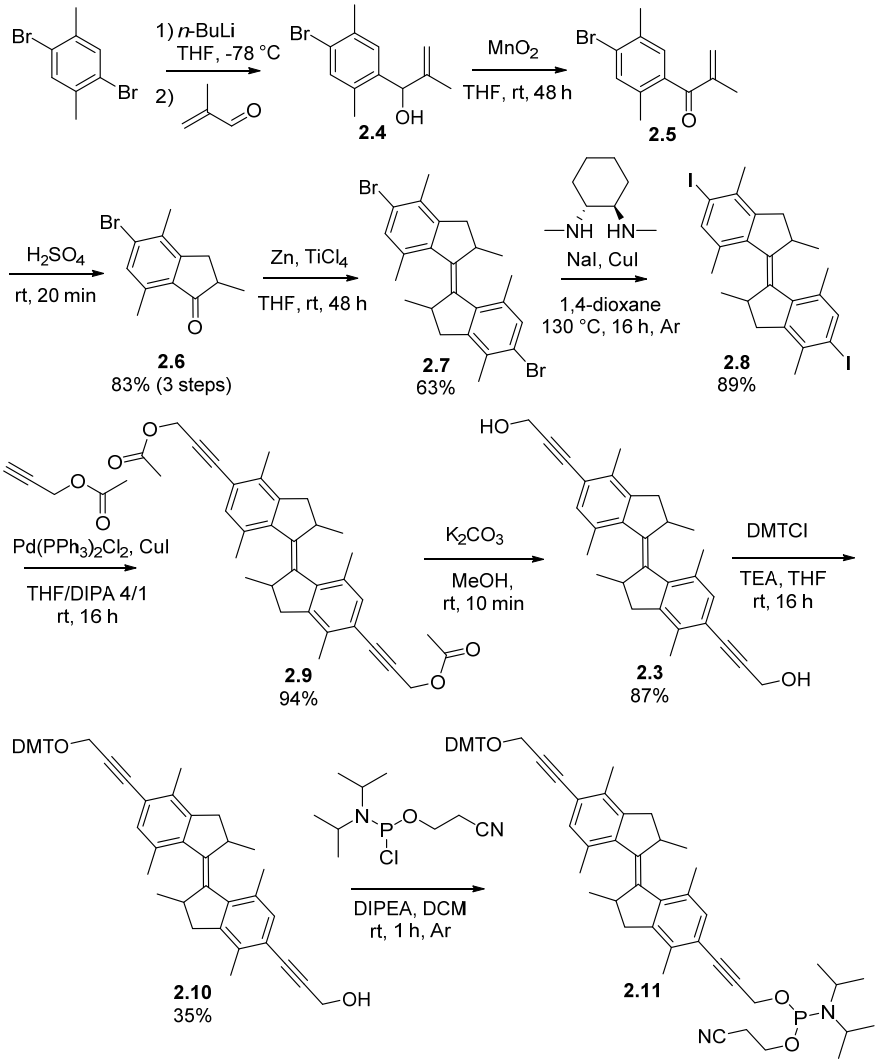

Scheme 2.2: Synthesis of motor **2.3** and phosphoramidite motor **2.11** (only *trans* isomer shown).

2.4 Analysis of the motor-based linker

2.4.1 ^{1}H NMR analysis

The thermal and photochemical steps in the rotation of molecular motor **2.3** were studied using ^{1}H NMR spectroscopy. Figure 2.3i shows the NMR spectrum of stable *trans*-**2.3** in CD_2Cl_2.[†]

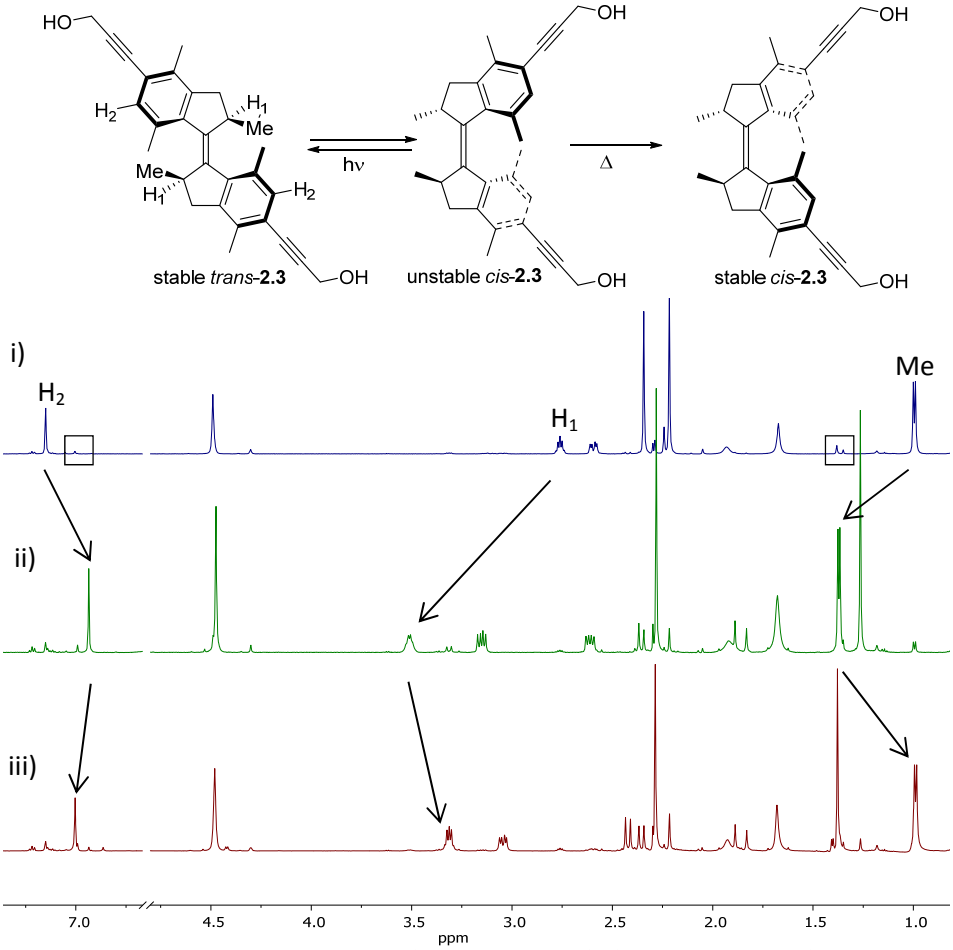

Figure 2.3: NMR experiments in CD_2Cl_2 (400 MHz, –50 °C). i) Stable *trans*-**2.3**, ii) PSS, reached after 15 h of irradiation (312 nm, –50 °C), iii) Sample after heating to 40 °C for 6 h, consisting mainly of stable *cis*-**2.3**. Some key signals are indicated. Boxes are used to indicate the signals corresponding to trace amounts of stable *cis*-**2.3**. For clarity, here and elsewhere in this thesis, only a single enantiomer of **2.3** is depicted, while the investigation was conducted on a racemic mixture unless otherwise indicated.

[†] As discussed previously, removing the *cis* isomer from the *trans* isomer did not succeed entirely (*vide supra*), therefore trace amounts of stable *cis*-**2.3** can be observed in Figure 2.3i.

The sample was cooled to –50 °C and irradiated with 312 nm light. The photostationary state (PSS, Figure 2.3ii) was reached after 15 h and consists of stable *trans*/unstable *cis* in a ratio of 12:88. Unstable *cis*-**2.3** was fully converted to stable *cis*-**2.3** by heating the sample to 40 °C for 6 h (iii).

Figure 2.4i shows the ^{1}H NMR spectrum of stable *cis*-**2.3** in CD_2Cl_2.

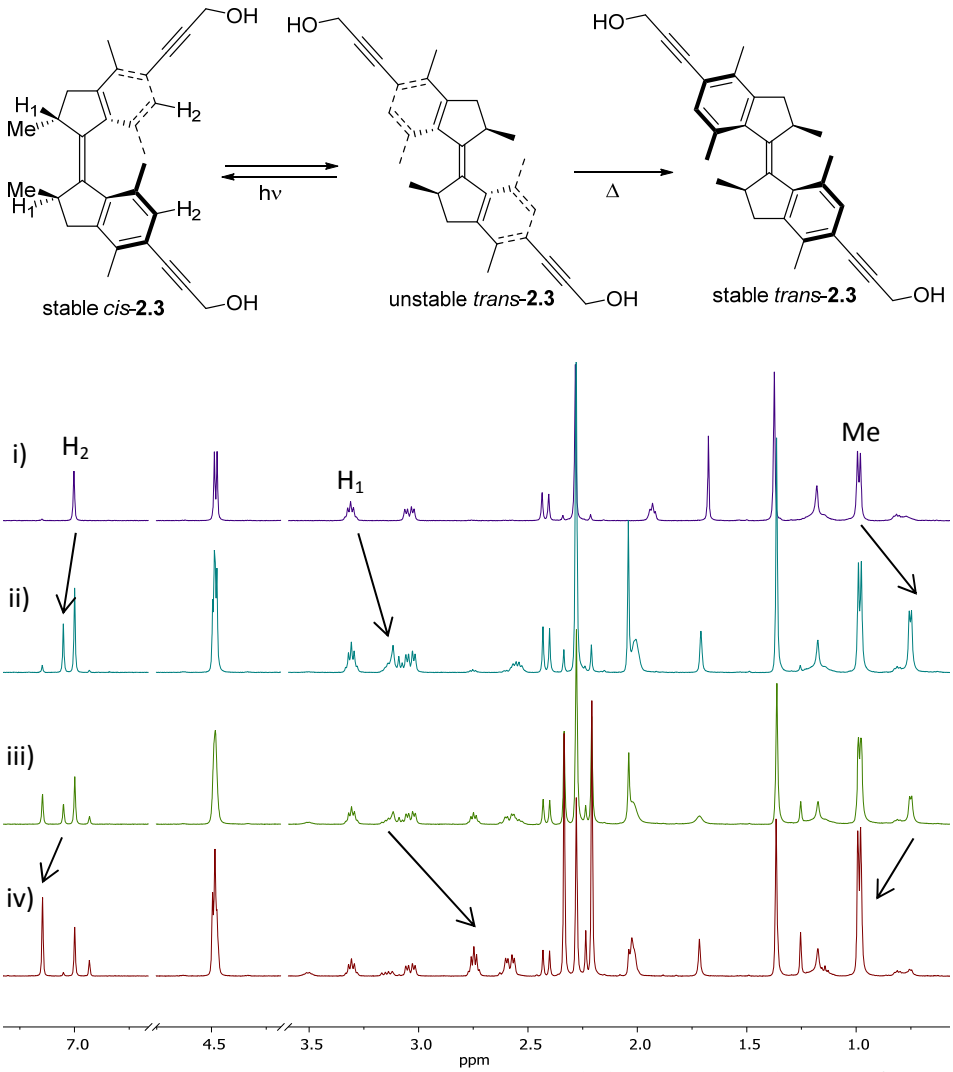

Figure 2.4: NMR experiments in CD_2Cl_2 (400 MHz, –50 °C). i) Stable *cis*-**2.3**, ii) Sample after 1 h of irradiation (312 nm, –50 °C), iii) Sample after 2.5 h of irradiation (312 nm, –50 °C), iv) Sample after heating to rt for 10 min. Some key signals are indicated.

The sample was cooled to –50 °C and irradiated with 312 nm light. After 1h, 40% conversion towards unstable *trans* was observed (Figure 2.4ii). Despite the very low tem-

perature, a small percentage of this unstable *trans* isomer has already undergone thermal helix inversion, and a small amount of stable *cis* isomer can be seen. The irradiation was continued for an additional 90 min (Figure 2.4iii), leading to a total of 55% conversion and a mixture of all four isomers. Unstable *trans*-**2.3** was fully converted to stable *trans*-**2.3** by heating the sample to rt for 10 min (Figure 2.4iv). These NMR experiments support our decision not to utilize unstable *trans*-**2.3**, since thermal helix inversion readily occurs even at -50 °C.

2.4.2 UV-vis analysis

The photochemical properties of motor **2.3** were studied using UV-vis spectroscopy. A $2 \cdot 10^{-5}$ M solution of motor *trans*-**2.3** was prepared in DCM and purged with argon. Because *trans*-**2.3** could not be isolated (*vide supra*), < 5% stable *cis* isomer was present. A UV-vis spectrum was recorded (Figure 2.5a, black line). The sample was irradiated with 312 nm light at 20 °C. The irradiation caused the major absorption band (λ_{max} = 328 nm) to decrease. Simultaneously, a new band appeared at 373 nm. This bathochromic shift is in accordance with formation of a higher energy isomer (unstable *cis*-**2.3**). The PSS was reached within 1 min and irradiation was halted. Subsequently, the sample was irradiated with 395 nm light (Figure 2.5b) to induce the reverse photochemical reaction (unstable *cis* to stable *trans*). After 4 min, the PSS was reached, indicating an almost complete reversal to stable *trans*-**2.3**.

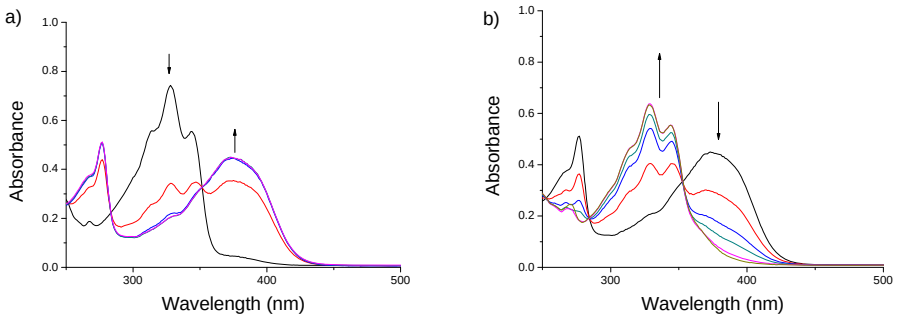

Figure 2.5: UV-vis spectra of analysis of the photochemical isomerization of stable *trans*-**2.3**. (a) Changes of the absorption spectrum of stable *trans*-**2.3** upon irradiation with 312 nm light. (b) Changes of the absorption spectrum of (a) upon irradiation with 395 nm light. All spectra recorded in DCM, rt, Ar.

2.4.3 Kinetic analysis

A $2 \cdot 10^{-5}$ M solution of motor *trans*-**2.3** was prepared in dichloroethane and the solution was purged with argon. Samples were prepared in quartz cuvettes (l = 1 cm). Samples were irradiated with 312 nm light at 20 °C, until the PSS was reached. The absorption at 380 nm was then measured over time until the thermal process was complete. All

exponential decay lines were fitted using least squares. The results were processed using a direct Eyring analysis with errors obtained by a Monte Carlo experiment. Table 2.1 lists the activation parameters and half life of the unstable *cis* isomer. The Eyring plot is depicted in Figure 2.6. The half life of the unstable *trans* isomer of xylene based first generation molecular motors is typically around 10 s at rt.[22] Because the target DNA hybrid is to be employed at physiological temperature, motor **2.3** can be seen as a three state switch. Therefore, the kinetic parameters of the thermal helix inversion from unstable *trans* to stable *trans* were not investigated.

	$t_{1/2}$ at 20 °C	$t_{1/2}$ at 37 °C	$\Delta^{\ddagger}G°$ (kJ/mol)	$\Delta^{\ddagger}H°$ (kJ/mol)	$\Delta^{\ddagger}S°$ (J/K/mol)
Unstable *cis* to stable *cis*	90.3 h ± 5.22	9.7 h ± 0.3	103.6 ± 0.1	96.5 ± 1.3	-24.0 ± 3.9

Table 2.1: Activation parameters and half-lives calculated for motor **2.3**.

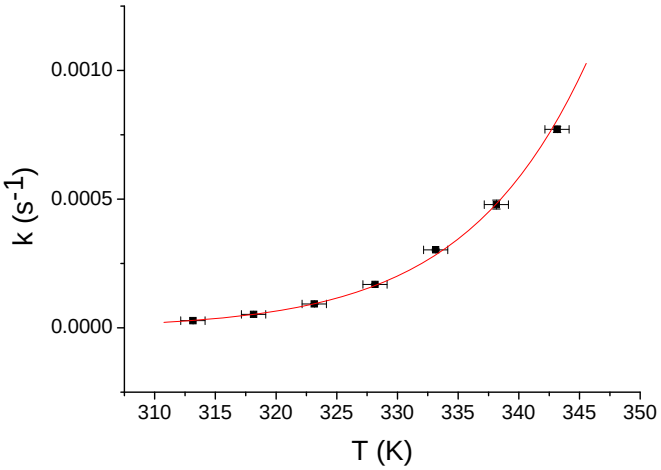

Figure 2.6: Eyring plot for the thermal helix inversion from unstable *cis*-**2.3** to stable *cis*-**2.3**.

2.5 DNA synthesis

Molecular motor building block **2.11** was introduced into a 16-mer, self-complementary DNA strand using standard solid phase oligonucleotide synthesis on a DNA synthesizer. *Cis* and *trans* isomers were synthesized separately from stable *cis*-**2.11** and *trans*-**2.11**, respectively. The product, 5'-TTTTTTTT-**2.3**-AAAAAAAA-3' (8T-**2.3**-8A), was purified using reversed phase chromatography followed by anion exchange chromatography. Product identity was confirmed by MALDI-TOF mass spectrometry (Mw calc=5361g/mol, Mw found=5348g/mol and 5349g/mol for 8T-*cis*-**2.3**-8A and for 8T-*trans*-**2.3**-8A, respectively). Duplex formation of two molecules 8T-**2.3**-8A was not

expected, since this was found to be extremely unfavourable for related oligonucleotides with stilbene backbone linkers.[16] Figure 2.7 shows gel images of several DNA samples. The positions of 8A8T (HY) (lane 5) is slightly lower than the 10bp band from the ladder, which means that this self-complementary DNA forms an intramolecular hairpin structure in buffer instead of hybridization between 2 strands. Meanwhile, for both *cis* and *trans*-**2.3** modified DNAs (lane 6 and lane 7), the electrophoretic mobilities of the major bands are lower than the unmodified 8A8T DNA (lane 5) while higher than the 15bp band from the ladder, which means the majority of both *cis* and *trans*-**2.3** modified DNAs form an intramolecular hairpin structure as well. Their slightly decreased mobility compared to 8A8T can be attributed to the introduction of the motor. When DNA is modified with hydrophobic polymer units, mobilities are also reduced compared to pristine DNA.[25] The minor bands for both motor DNAs could be attributed to intermolecular DNA duplexes.

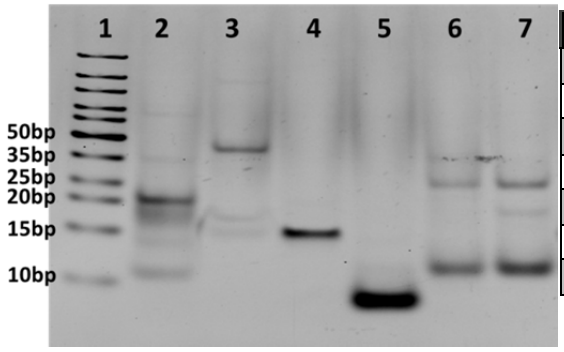

Lane	Sample
1	DNA ladder
2	16A
3	16T
4	16A+16T (HY)
5	8A8T (HY)
6	8T-*cis*-**2.3**-8A
7	8T-*trans*-**2.3**-8A

Figure 2.7: Polyacrylamide Gel Electrophoresis of various DNA samples. (HY) = DNA was hybridized prior to running gel.

2.6 Melting temperature analysis

The melting temperature of each hairpin was determined using a SYBR Green I fluorescence assay (Figure 2.8). The melting temperature for 8T-*cis*-**2.3**-8A was determined to be 59 °C, and for 8T-*trans*-**2.3**-8A to be 65 °C. The ΔT_m is therefore 6 °C, which is a remarkably high value and comparable to or even surpassing the achievement of Sugimoto and co-workers (20 °C for 5 bp, 13.9 °C for 6 bp).[19,20] Comparison with an 8 bp DNA hairpin containing an azobenzene or stilbene linker is not possible. Only three such hybrids were previously reported, and a ΔT_m was not reported for any of them.[26–28] Notably, the T_m of the native hairpin 8T8A was determined to be 51.5 °C. The observation that the T_m of the native hairpin is lower than the T_m of the hybrids can be partly attributed to the fact that the loop in this hairpin consists of a few bases, which are therefore not engaging in base pairing. Typically, a four nucleotide loop is found to be most stable.[29] The loss of two base pair interactions is expected to decrease the T_m a few degrees, while the T_m's of 8T-*cis*-**2.3**-8A and 8T-*trans*-**2.3**-8A are, respectively, 7.5 °C

and 13.5 °C higher than the T_m of 8T8A. It seems therefore that for both isomers, the motor has a significant stabilizing effect on the hairpin. A similar stabilizing effect is observed for *trans* azobenzenes and stilbenes, where it has been attributed to π stacking interactions.[11,30]

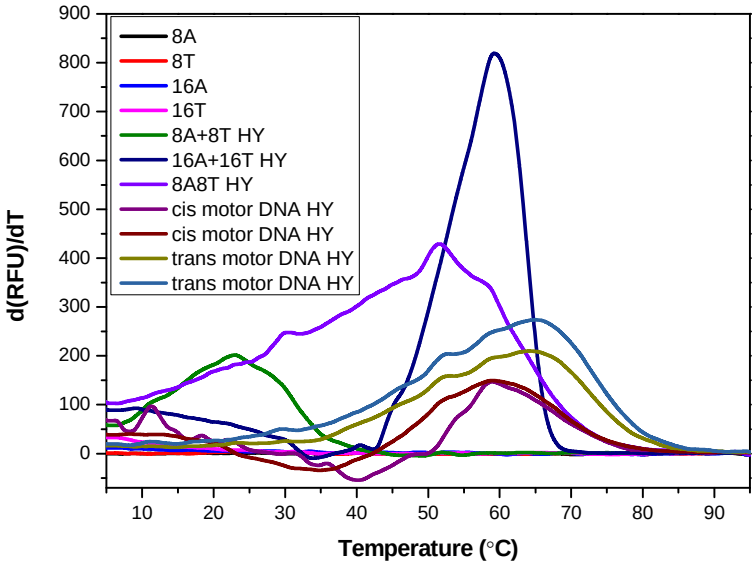

Figure 2.8: First derivatives of fluorescence of SYBR Green I in the presence of various DNA samples. (HY) = DNA was hybridized prior to recording melting curves.

2.7 DNA photochemistry

To achieve photocontrol over DNA secondary structure, it is very important that the switching ability of the motor in the hybrid is retained. A 2.65 µM solution of 8T-*trans*-**2.3**-8A in Milli-Q water was subjected to the standard UV-vis experiment used to follow the isomerization processes of a molecular motor (Figure 2.9). In the initial absorption spectrum (Figure 2.9a, b, black line) both components of the hybrid can be clearly distinguished. The major absorption band can be attributed to DNA (λ_{max} = 262 nm), while above ~300 nm, only the motor units contribute to absorption. The band with two maxima at λ_{max} = 330 and 345 nm is characteristic for the stable *trans* conformation of xylene-based first generation motors[22,31,32] and is also observed in the UV-vis spectrum of motor **2.3** (Figure 2.5). Because the DNA does not absorb above 300 nm, the motor unit can be irradiated without affecting the DNA part of the hybrid. Irradiation with 312 nm leads to the appearance of a new absorption band at a higher wavelength (λ_{max} = 385 nm), which typically results from the formation of a higher energy motor isomer (8T-unstable-*cis*-**2.3**-8A, Figure 2.9a). The clear isosbestic point indicates the absence of photodamage or side reactions. After 10 min, a photostationary state was

reached and the irradiation was halted (Figure 2.9b, red line). Subsequently, the sample was left at 67 °C for several hours to induce thermal helix inversion. As expected, the new band disappeared and an absorption at lower wavelength (λ_{max} =347 nm, Figure 2.9b, blue line) appeared, most likely a band corresponding to 8T-*cis*-**2.3**-8A. Separation of the two isomers of 8T-**3**-8A could not be found using chromatography, and too little material was available to attempt characterization through NMR spectroscopy. However, MALDI-TOF analysis showed that the hybrid does not undergo degradation.

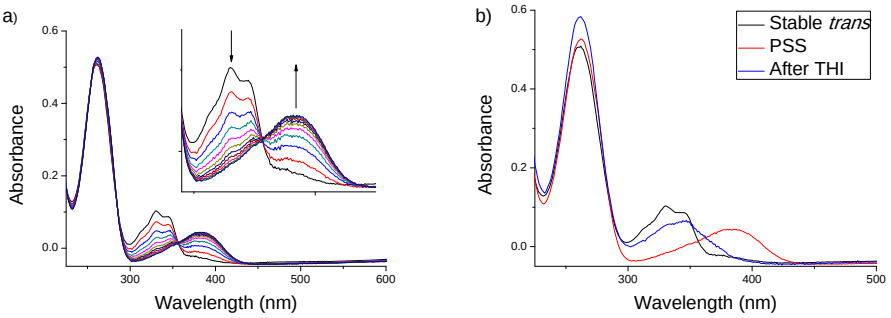

Figure 2.9: UV-vis spectra of analysis of the photochemical isomerization of stable 8T-*trans*-**2.3**-8A. (a) Changes of the absorption spectrum of 8T-*trans*-**2.3**-8A upon irradiation with 312 nm light. Insert shows the region 290-450 nm.(b) 8T-*trans*-**2.3**-8A (black line), the sample after irradiation with 312 nm light for 10 min (red line) and the sample after incubation at 67 °C for 6 h (blue line). All spectra recorded in Milli-Q, 67 °C, ambient atmosphere.

Although the UV-vis spectra alone clearly indicate a photoisomerization followed by THI, the sample used in this experiment was subjected to a melting temperature analysis by a fluorescence assay. It was hypothesized that a mixture of the two hairpins (8T-*trans*-**2.3**-8A and 8T-*cis*-**2.3**-8A) should lead to two maxima in the differentiated curve of the fluorescence spectrum, corresponding to the two different T_m's. In fact, the main maximum in this curve was found at 59 °C, which corresponds to the T_m of 8T-*cis*-**2.3**-8A (Figure 2.10a). This result, in combination with the UV-vis spectra depicted in Figure 2.9, leads us to conclude that an efficient photoisomerization and subsequent THI have taken place. To determine the kinetics of the THI, the absorption of the sample was measured at regular intervals (Figure 2.10ba). The half-life of the unstable *cis* isomer of 8T-**2.3**-8A is determined to be ~51 min at 67 °C, about 2.5 x slower than for the motor **2.3** itself (*vide supra*, 19.5 min at 67 °C).

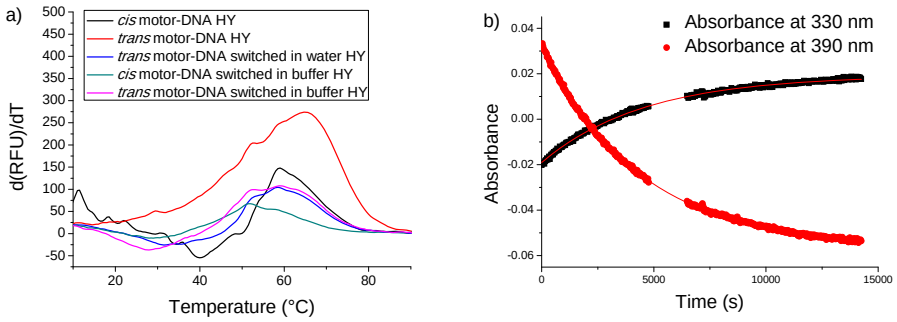

Figure 2.10: (a) First derivatives of fluorescence of SYBR Green I in the presence of various DNA samples after irradiation. (HY) = DNA was hybridized prior to recording melting curves. (b) Change in absorbance over time of 8T-**2.3**-8A. The sample (8T-*trans*-**2.3**-8A, 2.65 µL, Milli-Q) was first irradiated at 312 nm for 10 min at 67 °C. Subsequently the sample was left to undergo THI. Depicted here is the absorbance at 330 nm (black squares) and 390 nm (red circles) and their respective fitted exponential decay curves. A small time window is taken out due to artefacts.

The experiment was also performed under hybridizing conditions at physiological temperature (37 °C, 20mM Tris-HCl, 100mM NaCl, 10mM $MgCl_2$, pH 8.0). 8T-*Trans*-**2.3**-8A was again readily photoisomerized without the occurrence of side reactions (Figure 2.11a). However, after several hours at 37 °C, only a slight decrease of the absorption band corresponding to the unstable *cis* isomer was observed (Figure 2.11b). Potentially, helix inversion is hindered by the hybridized DNA strands. When the sample was heated to 70 °C (above the T_m), THI occurred in a similar manner in aqueous buffer as in water. MALDI-TOF analysis of the irradiated sample revealed that no significant degradation had taken place. Melting temperature analysis revealed a T_m of 59 °C, indicating efficient conversion to the stable *cis* isomer (Figure 2.10a).

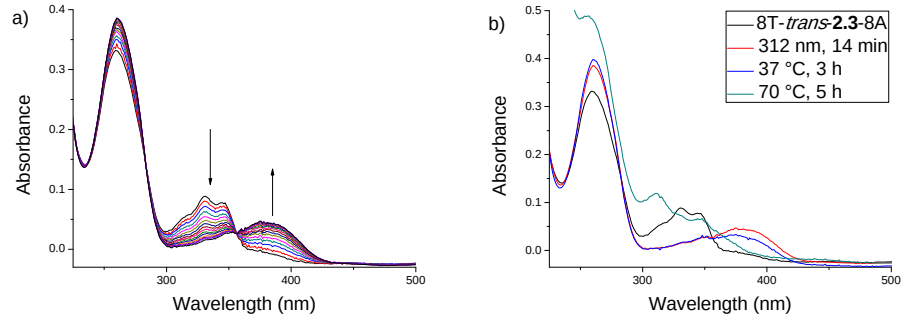

Figure 2.11: UV-vis spectra of analysis of the photochemical isomerization of stable 8T-*trans*-**2.3**-8A in aqueous buffer. (a) Changes of the absorption spectrum of 8T-*trans*-**2.3**-8A upon irradiation with 312 nm light. (b) 8T-*trans*-**2.3**-8A (black line), the sample after irradiation with 312 nm light for 14 min (red line) the sample after incubation at 37 °C for 3 h (blue line) and the sample after incubation at 70 °C for 5 h (turquoise line). All spectra were recorded in Tris buffer, pH = 8, 37 °C, at ambient atmosphere.

Combining the results of the UV-vis and melting temperature experiments, Figure 2.12 gives a schematic overview of the operation of 8T-**2.3**-8A. Stable 8T-*trans*-**2.3**-8A (left) forms a hairpin structure with a T_m of 65 °C. Upon irradiation with 312 nm light, photoisomerization to unstable 8T-*cis*-**2.3**-8A (middle) occurs with high conversion. Upon heating, THI can be induced and stable 8T-*cis*-**2.3**-8A (right) is formed. The T_m of this isomer is 59 °C, indicating a destabilization of the hairpin structure.

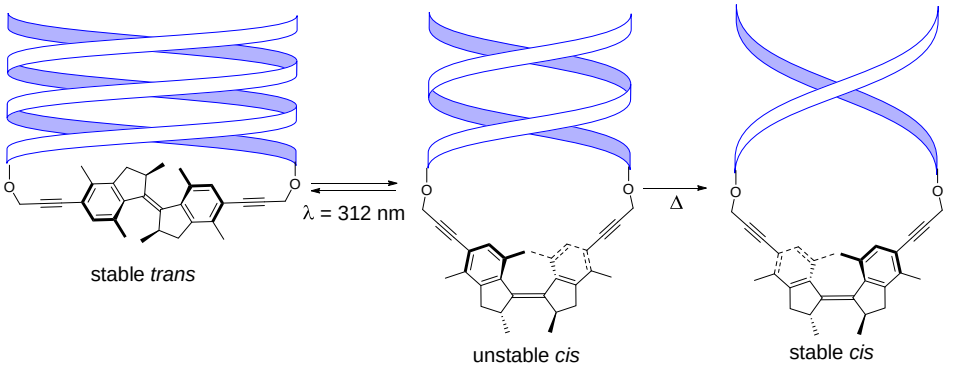

Figure 2.12: Schematic overview of the functioning of 8T-**2.3**-8A. *Trans-cis* isomerization leads to a destabilization of the helix, as is apparent from the decrease in T_m. For clarity, the destabilization is represented by partial helix unwinding in this figure.

The half-life of unstable *trans*-**2.3** is estimated to be extremely short (*vide supra*). However, with 8T-*cis*-**2.3**-8A in hand, a study of the photoisomerization was attempted anyway. Upon irradiation with 312 nm light at 37 °C, a very small change in the UV-vis spectrum can be observed (Figure 2.13a). The appearance of a higher wavelength absorbance band and a clear isosbestic point suggest photoisomerization towards the unstable *trans* isomer, and a relatively long half-life of this isomer.

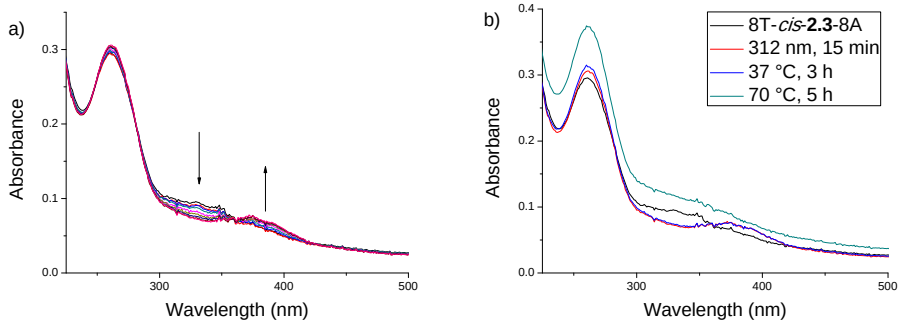

Figure 2.13: UV-vis spectra of analysis of the photochemical isomerization of stable 8T-*cis*-**2.3**-8A in aqueous buffer. (a) Changes of the absorption spectrum of 8T-*cis*-**2.3**-8A upon irradiation with 312 nm light. (b) 8T-*cis*-**2.3**-8A (black line), the sample after irradiation with 312 nm light for 15 min (red line) the sample after incubation at 37 °C for 3 h (blue line) and the sample after incubation at 70 °C for 5 h (turquoise line). All spectra recorded in Tris buffer, pH = 8, 37 °C, ambient atmosphere.

Similar to the other half of the cycle, leaving the sample for several hours at 37 °C did not cause any significant change to the spectrum (Figure 2.13b). The sample was subsequently heated to 70 °C for several hours. Although the shape of the spectrum indicates the occurrence of a thermal process, severe baseline shifts prevent any quantitative analysis. MALDI-TOF analysis was used to rule out degradation.

The results of the unstable *trans* isomer of 8T-**2.3**-8A are not unexpected, since due to the short half-life of the unstable *trans* isomer various thermal and photochemical processes may be occurring simultaneously. However, the photoisomerization and subsequent THI of 8T-stable-*trans*-**2.3**-8A towards 8T-stable-*cis*-**2.3**-8A occur without degradation. Although the elevation to a temperature above the T_m is required to induce THI, the photoisomerization occurs readily under hybridizing conditions and at physiological temperature.

2.8 Molecular Dynamics

As discussed above, bridgehead motor **2.3** was carefully designed to ensure an optimal geometrical change upon *cis-trans* isomerization. Intriguingly, in sharp contrast to predictions based on our design, 8T-*trans*-**2.3**-8A proved to have a higher T_m than 8T-*cis*-**2.3**-8A, since DFT calculations suggested the reverse. However, the DFT calculations were only performed on the motor bridgehead, and artificial contraction was used to simulate a DNA hairpin attached to the oxygen atoms. A DFT study of the full hairpin was not considered feasible, due to the excessive computational time such an investigation would require. To explain the difference in hairpin stability, preliminary Molecular Dynamics (MD) simulations were performed, exploring the conformations that the stable *cis* and *trans* conformers can adopt. The simulations used the well-known AMBER force field for DNA and that model was extended to include the linker moiety. Native B-DNA hairpin structures were built and bridged by linker **2.3** in either *cis* or *trans* isomer. Water and counter ions were added. Briefly, the hairpin was observed to remain largely intact, but in both isomers, the base pair closest to the linker was observed to be able to adopt multiple conformations. These include base-flips and stacking of two bases of the first pair on top of each other, apparently engaging in stacking interactions with one of the aromatic rings of the motor. Selected snapshots from the observed conformations are shown in Figure 2.14. The simulations allow speculation as to the reasons why the *trans* form of 8T-**2.3**-8A is more stable than the *cis* form (see caption to Figure 2.14). For example, stacking interactions between the bases and the motor may be possible. However, these preliminary simulations (90 ns) are much too short to allow quantitative statements. Extensive simulations should result in the determination the free energy differences between the different types of conformations and thereby give insight into the relative stability of the hairpin; investigations that are currently underway.

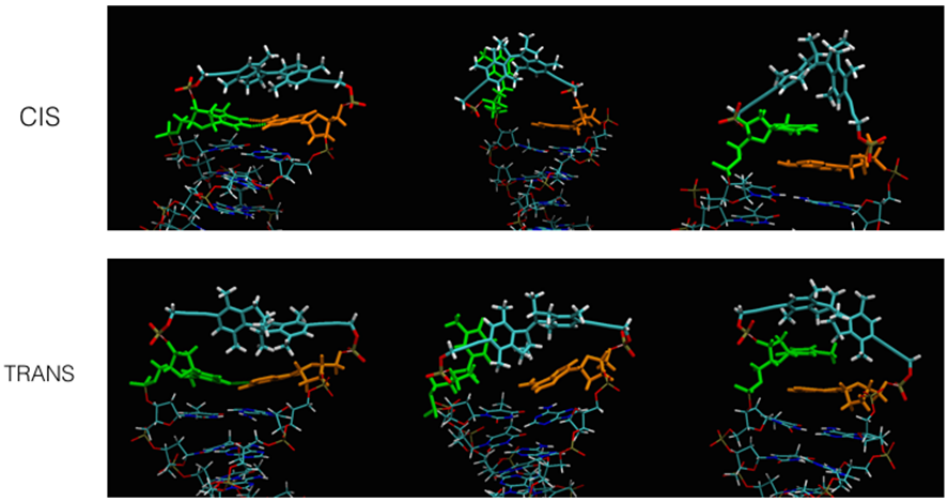

Figure 2.14: Selected conformations taken from 90 ns MD simulations of hairpin constructs with the linker in the stable *cis* (top) and *trans* (bottom) conformations, respectively. The molecule is visualized using the VMD software, highlighting the switchable bridge (cyan C-atoms), the adenine at the 5' end (orange) and the 3' thymine (green). H-bonding interactions defined on the basis of the Luzar-Chandler-geometric criterion (donor-acceptor distance within 3.5 Å and donor-H-acceptor angle smaller than 30 degrees) between the two selected base pairs are shown as dashed lines. Left: the starting conformation with canonical base pairing, obtained after building and briefly equilibrating the model. Middle: structures with the thymine neighbouring the switchable bridge bases flipped out of the hairpin are shown. Right: structures in which the base pairs closest to the switchable bridge have stacking interactions instead of base-pairing interaction. In the *trans* form (right bottom), the thymine appears to be interacting also favourably with one of the aromatic moieties of the switchable linker; this interaction is possibly less favourable in the *cis* form.

2.9 Conclusions

Aided by computational studies, a first generation molecular motor-based linker was designed, that can function as a photoswitchable bridgehead for an 8 base pair DNA hairpin. Both *cis* and *trans* isomers of a bifunctional linker were prepared and, after establishing their function as a multistate switch, they were incorporated in a 16-mer strand of self-complementary DNA *via* solid phase synthesis. Hairpin formation was confirmed, and the DNA-motor hybrid was shown to be able to undergo both photoisomerization and thermal helix inversion processes. The T_m of 8T-*trans*-**2.3**-8A was determined to be 65 °C, and the T_m of 8T-*cis*-**2.3**-8A was 59 °C. An unexpected observation was the destabilization due to *trans-cis* isomerization, since DFT calculations suggested the opposite. However, more extensive MD investigations will provide better insight into the interactions between the hairpin and the photoswitchable bridgehead. The results and structural insights of this study are very important for the design of even more potent molecular motor-backbone linkers. The measured ΔT_m of 6 °C (for an 8 bp hairpin) represents a very promising value which ranks this investigation among the most successful attempts to influence DNA hybridization through the incorporation of a

photoswitchable backbone linker. Moreover, the isomerization process was highly efficient, and the bistable switching mode provides a real advance over azobenzenes, for which the thermal *cis-trans* reisomerisation limits possible applications. This study marks the first time that a molecular motor has been used to control the secondary structure of DNA, and in fact one of the first examples of a molecular motor being applied under physiological conditions, demonstrating the ability to regulate a key biological process such as DNA hybridization to a great extent.

Finally, it must be noted that molecular motors do not just rival conventional photoswitches in efficiency and power. They also offer a much higher degree of control and precision due to their four state switching cycle and helicity inversion. This investigation has only begun to uncover the vast range of new possibilities that may be accessed in photoregulated biohybrid systems. It is apparent that the motor unit by itself is powerful enough to significantly influence hybridization behaviour of short oligonucleotide hairpins. Moreover, our results showcase the potential of rotary molecular motors and consolidate their position among the most effective photoswitches for use in biological surroundings.

2.10 Experimental procedures and acknowledgements

DNA synthesis, gel electrophoresis, MALDI-TOF mass analysis and melting temperature analysis were performed by Qing Liu. Initial investigation into DNA synthesis were performed by Jan Willem de Vries. Zhuojun Meng assisted with melting temperature analysis. DFT calculations were performed by Jos Kistemaker. Preliminary MD investigations were conducted by Alex de Vries and Ignacio Faustino. Dowine de Bruijn is gratefully acknowledged for valuable discussions.

General Remarks

Chemicals were purchased from Sigma Aldrich, Acros or TCI Europe N.V.; solvents were reagent grade and distilled and dried before use according to standard procedures, if required. Column chromatography was performed on silica gel (Silica Flash P60, 230–400 mesh). ^{1}H, ^{13}C and ^{31}P -NMR spectra were recorded on a Varian Gemini-200 (50 MHz), a Varian AMX400 (101 MHz), or a Varian Inova (500, 125 MHz). Chemical shifts are denoted in δ values (ppm) relative to $CHCl_3$ (^{1}H: δ = 7.26 and ^{13}C: δ = 77.16), $CDHCl_2$ (^{1}H: δ = 5.32 and ^{13}C: δ = 53.84), DMSO-d5 (^{1}H: δ = 2.50 and ^{13}C: δ = 39.52), DMF-d6 (^{1}H: δ = 8.03, 2.92, 2.75 and ^{13}C: δ = 163.15, 34.89, 29.76), DHO (^{1}H: δ = 4.79), CD_2HCN (^{1}H: δ = 1.94 and ^{13}C: δ = 118.26, 1.32) or CD_3OD (^{1}H: δ = 3.31 and ^{13}C: δ = 49.00). For ^{1}H-NMR, the splitting parameters are designated as follows: s (singlet), d (doublet), t (triplet), q (quartet), p (pentet), h (heptet), m (multiplet) and app (apparent). HRMS spectra were recorded on a Thermo Fischer Scientific Orbitrap XL with ESI, APPI and/or APCI ionization sources. Melting points are taken on a Büchi B-545 melting point apparatus. UV-vis absorption spectra were measured on a Jasco V-

630 spectrometer. Irradiation was performed using a Spectroline ENB-280C/FE lamp (312 or 365 nm). All solvents and reagents for oligonucleotide synthesis were purchased from Novabiochem (Merck, UK) and SAFC (Sigma-Aldrich, Netherlands). Solid supports (Primer SupportTM, 33 µmol/g) from Glen Research were used for the synthesis of motor-DNA. The motor-DNA's were characterized by MALDI-TOF mass spectrometry using a 3-hydroxypicolinic acid matrix. Spectra were recorded on an ABI Voyager DE-PRO MALDI TOF (delayed extraction reflector) Biospectrometry Workstation mass spectrometer. All unmodified oligonucleotides were purchased from Biomers.net in HPLC purification grade.

1-(4-bromo-2,5-dimethylphenyl)-2-methylprop-2-en-1-ol (2.4)

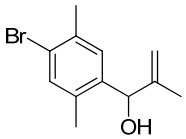

2,5-Dibromo-*p*-xylene (1.0 g, 3.8 mmol) was dissolved in THF (25 mL) and cooled to -78 °C under a nitrogen atmosphere. *n*-BuLi (1.6 M solution in hexane, 2.5 mL, 4.0 mmol) was added dropwise and the reaction mixture was stirred for 20 min at -78 °C. Methacrolein (630 µL, 7.60 mmol) was added dropwise and the reaction mixture was stirred for 1 h, after which the flask was allowed to warm up to room temperature under continuous stirring. The reaction was quenched with water (10 mL) and a drop of HCl (aq.). The reaction mixture was extracted with ether (2 x 25 mL) and DCM (1 x 25 mL). The combined organic layers were dried over Mg_2SO_4, filtered and concentrated *in vacuo*. ^{1}H NMR (400 MHz, $CDCl_3$) δ 7.32 (s, 1H), 7.29 (s, 1H), 5.23 (s, 1H), 5.11 (s, 1H), 5.00 (s, 1H), 2.36 (s, 3H), 2.27 (s, 3H), 1.82 (s, 1H), 1.63 (s, 3H). ^{13}C NMR (101 MHz, $CDCl_3$) δ 145.9, 139.1, 135.5, 135.3, 134.1, 128.8, 123.9, 112.4, 74.2, 22.7, 19.0, 18.6; mp = 62 °C; HRMS (ESI): *m/z* calcd for $C_{12}H_{14}Br$: 237.02625, found 237.02734 ($M-H_2O$).

1-(4-bromo-2,5-dimethylphenyl)-2-methylprop-2-en-1-one (2.5)

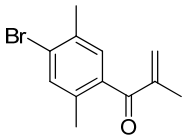

Compound **2.4** was dissolved in THF (25 mL) and MnO_2 (3.3 g, 38 mmol) was added. The reaction was stirred at room temperature over weekend. After 24 h, additional MnO_2 (1.7 g, 17 mmol) was added. The reaction mixture was subsequently filtered over celite and evaporated to dryness. **2.5** was obtained as a pale yellow oil. ^{1}H NMR (400 MHz, $CDCl_3$) δ 7.40 (s, 1H), 7.08 (s, 1H), 5.97 (s, 1H), 5.58 (s, 1H), 2.36 (s, 3H), 2.22 (s, 3H), 2.03 (s, 3H); ^{13}C NMR (50 MHz, $CDCl_3$) δ 199.7, 145.0, 138.1, 135.2, 134.6, 134.2, 130.0, 129.8, 126.2, 22.3, 18.9, 17.2; HRMS (ESI): *m/z* calcd for $C_{12}H_{14}BrO$: 253.02225, found 253.02127.

5-bromo-2,4,7-trimethyl-2,3-dihydro-1H-inden-1-one (2.6)

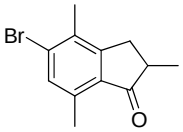

2.5 was dissolved in H_2SO_4 (10 mL) and stirred at room temperature for 20 min. Upon completion the reaction was quenched on ice. The solution was extracted with diethyl ether (3 x 25 mL). The combined organic layers were washed with a saturated aqueous $NaHCO_3$ solution (25 mL) and brine (25 mL), dried over Mg_2SO_4, filtered and concentrated *in vacuo*. The product was purified by flash column chromatography (SiO_2, 1% Et_2O in pentane). **2.6** was obtained as a white solid in 83% yield (797.7 mg, 3.154 mmol). ^{1}H NMR (400 MHz, $CDCl_3$) δ 7.34 (s, 1H), 3.28 (dd, *J* = 17.2, 7.9 Hz, 1H), 2.66 – 2.68 (m, 1H), 2.62 – 2.54 (m, 4H), 2.35 (s, 3H), 1.30 (d, *J* = 7.4 Hz, 3H); ^{13}C NMR (50 MHz, $CDCl_3$) δ 210.0, 154.5, 137.5, 133.0, 132.8, 131.6, 42.6, 34.6, 17.9, 17.8, 16.7; mp 77.9-78.2 °C; HRMS (APCI): *m/z* calcd for $C_{12}H_{13}OBr$: 253.0223, found 253.0229.

5,5'-dibromo-2,2',4,4',7,7'-hexamethyl-2,2',3,3'-tetrahydro-1,1'-biindenylidene (2.7)

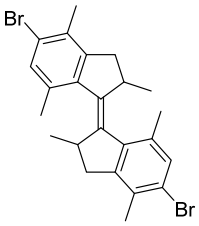

$TiCl_4$ (3.8 mL, 35 mmol) was added dropwise to a stirred suspension of Zn (4.56 g, 70.3 mmol) in THF (36 mL) at 0 °C under a nitrogen atmosphere. The mixture was heated at reflux for 2 h in an oil bath. Ketone **2.6** (4.45 g, 17.6 mmol) was added and the mixture was stirred for 72 h at reflux. The mixture was then cooled down to room temperature and filtered through a plug of SiO_2. The remaining tar-like substance in the flask was dissolved in ethyl acetate and also poured on the filter. The SiO_2 was washed with diethyl ether (3 x 200 mL) and the combined organic layers were dried ($MgSO_4$), filtered and concentrated *in vacuo*. The crude product was purified using flash column chromatography (SiO_2, pentane, R_f = 0.95). Motor **2.7** was obtained as a white solid, in a 1: 1.2 mixture of *cis* and *trans* isomers (2.63 g, 5.54 mmol, 63%) Isomers could be separated through recrystallization from heptane and subsequent crystal picking. *Cis*-**2.7** crystallizes as needles whereas *trans*-**2.7** crystallizes as cubes. *Cis* ^{1}H NMR (400 MHz, $CDCl_3$) δ 7.16 (s, 1H), 3.32 (app. p, 1H), 3.13 (dd, *J* = 15.0, 6.2 Hz, 1H), 2.48 (d, *J* = 15.0 Hz, 1H), 2.32 (s, 3H), 1.49 (s, 3H), 1.06 (d, *J* = 6.7 Hz, 3H); ^{13}C NMR (101 MHz, $CDCl_3$) δ 145.9, 140.3, 140.0, 134.6, 131.5, 130.5, 123.5, 41.8, 39.9, 20.3, 20.3, 18.6; mp = 204.3-204.7 °C. *Trans* ^{1}H NMR (400 MHz, $CDCl_3$) δ 7.30 (s, 2H), 2.83 (app. p, 2H), 2.70 (dd, *J* = 14.6, 5.7 Hz, 2H), 2.39 (s, 3H), 2.27 (app. d, 8H), 1.07 (d, *J* = 6.4 Hz, 6H); ^{13}C NMR (101 MHz, $CDCl_3$) δ 144.5, 141.3, 140.3, 132.9, 132.2, 131.4, 123.6, 42.3, 40.2, 21.7, 19.4, 18.7; mp = 185 °C. HRMS (APPI): *m/z* calcd for $C_{36}H_{37}BrO_2$: 474.03753, found 474.03692.

5,5'-diiodo-2,2',4,4',7,7'-hexamethyl-2,2',3,3'-tetrahydro-1,1'-biindenylidene (2.8)

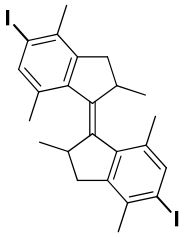

Motor **2.7** (1.49 g, 3.15 mmol), NaI (2.83 g, 18.90 mmol), CuI (90 mg, 0.47 mmol) and *N*,*N*'-dimethylethylene diamine (102 µl, 0.950 mmol) were mixed in a high pressure flask equipped with a magnetic stirrer. 1,4-Dioxane (15 mL, degassed by argon purging) was added and the reaction mixture was stirred and heated to 130 °C for 24 h under an argon atmosphere. After cooling to room temperature, water (15 mL) was added and the mixture was extracted with dichloromethane (3 x 20 mL). The combined organic layers were washed with brine (20 mL), dried over $MgSO_4$, filtered and concentrated *in vacuo*. The crude product was purified using flash column chromatography (SiO_2, pentane, R_f = 1). Motor **2.8** was obtained as a white solid, in a 1: 1.2 mixture of *cis* and *trans* isomers (1.59 g, 2.80 mmol, 89%). *Cis* ^{1}H NMR (400 MHz, $CDCl_3$) δ 7.44 (s, 2H), 3.29 (app. p, 2H), 3.13 (dd, J = 15.0, 6.4 Hz, 2H), 2.48 (d, J = 15.0 Hz, 2H), 2.35 (s, 6H), 1.46 (s, 6H), 1.06 (d, J = 6.8 Hz, 6H); ^{13}C NMR (101 MHz, $CDCl_3$) δ 144.9, 141.0, 140.7, 138.3, 135.0, 133.9, 100.3, 41.7, 40.4, 23.9, 20.3, 20.2; mp = 140 °C. *Trans* ^{1}H NMR (400 MHz, $CDCl_3$) δ 7.60 (s, 1H), 2.81 (app. p), 2.71 (dd, J = 14.6, 5.7 Hz, 1H), 2.37 (s, 3H), 2.29 (s, 3H), 1.07 (d, J = 6.4 Hz, 3H).^{13}C NMR (101 MHz, $CDCl_3$) δ 143.5, 141.5, 141.3, 139.0, 134.8, 133.3, 100.2, 42.2, 40.7, 23.9, 21.5, 19.4; no mp recorded because of presence of 5% *cis*-**2.8**. HRMS (APPI): *m/z* calcd for $C_{24}H_{26}I_2$: 568.0118, found 568.0112.

(2,2',4,4',7,7'-hexamethyl-2,2',3,3'-tetrahydro-[1,1'-biindenylidene]-5,5'-diyl)bis(prop-2-yne-3,1-diyl) diacetate (2.9)

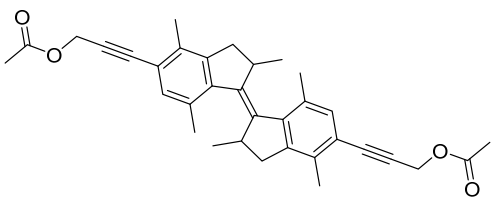

A 4:1 THF/DIPEA mixture was degassed by the freeze-pump-thaw method. Motor **2.8** (115 mg, 0.202 mmol), CuI (4 mg, 0.02 mmol) and $PdCl_2(PPh_3)_2$ (29 mg, 0.040 mmol) were dissolved in 3 mL of the solvent mixture and stirred at room temperature under a nitrogen atmosphere. After 15 min, propargyl acetate (198 µL, 2.04 mmol) was added dropwise. After 72 h, 5 mL of water was added. The mixture was extracted with ethyl acetate (3 x 5 mL). The combined organic layers were washed with brine (5 mL), dried over $MgSO_4$, filtered and concentrated *in vacuo*. The crude product was purified using flash column chromatography (SiO_2, pentane/diethyl ether). Motor **2.9** was obtained as a white solid, in a 1: 1.2 mixture of *cis* and *trans* isomers (95.1 mg, 0.187 mmol, 94%). The *cis* isomer could be isolated from the mixture by recrystallization from pentane and diethyl ether. *Cis* ^{1}H NMR (400 MHz, $CDCl_3$) δ 7.08 (s, 2H), 4.95 (s, 4H), 3.33 (dd, J = 13.1, 6.5 Hz, 2H), 3.08 (dd, J = 15.1, 6.3 Hz, 2H), 2.45 (d, J = 14.9 Hz, 2H), 2.34 (s, 6H), 2.12 (s, 6H), 1.45 (s, 6H), 1.05 (d, J = 6.7 Hz, 6H); ^{13}C NMR (101 MHz, $CDCl_3$) δ 170.5, 144.6, 141.8, 141.6, 133.2, 133.1, 132.5, 120.5, 86.4, 86.4, 53.3, 41.8, 39.2, 21.0, 20.5, 20.4, 16.8; mp = 139.6 °C. *Trans* ^{1}H NMR (400 MHz, $CDCl_3$) δ 7.22 (s, 2H), 4.95 (s,

4H), 2.83 (app. p, 2H), 2.64 (dd, *J* = 14.6, 5.7 Hz, 2H), 2.39 (s, 6H), 2.27 (s, 6H), 2.26 (d, *J* = 15.1 Hz, 2H), 2.13 (s, 6H), 1.05 (d, *J* = 6.4 Hz, 6H); ^{13}C NMR (101 MHz, $CDCl_3$) δ 170.6, 143.0, 142.2, 141.9, 133.9, 132.9, 131.1, 120.6, 86.3, 86.3, 53.3, 42.1, 39.4, 21.7, 21.1, 19.5, 16.7; mp not recorded due to presence of 5% *cis* isomer. HRMS (ESI):: *m/z* calcd for $C_{34}H_{37}O_4$: 509.2686, found 509.2658 ($M+H^+$).

3,3'-(2,2',4,4',7,7'-hexamethyl-2,2',3,3'-tetrahydro-[1,1'-biindenylidene]-5,5'-diyl)bis(prop-2-yn-1-ol) (2.3)

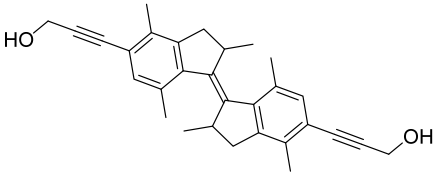

Motor *cis*-**2.9** (93.4 mg, 0.18 mmol) and K_2CO_3 (50.7 mg, 0.37 mmol) were dissolved in methanol (7 mL) and stirred at room temperature. After 10 min, 7 mL diethyl ether and 10% aq. KH_2PO_4 (7 mL) were added and the reaction mixture was vigorously stirred for 15 min. The reaction mixture was extracted with diethyl ether (3 x 15 mL). The combined organic layers were washed with brine (5 mL), dried over $MgSO_4$, filtered and concentrated *in vacuo*. No further purification was required. Motor *cis*-**2.3** was obtained as a white solid (68 mg, 0.16 mmol, 87%). Motor *trans*-**2.3** (a viscous yellow oil) could be obtained using the same procedure. *Cis* ^{1}H NMR (500 MHz, CD_2Cl_2) δ 7.04 (s, 2H), 4.52 (d, *J* = 6.4 Hz, 4H), 3.35 (p, *J* = 7.0 Hz, 2H), 3.08 (dd, *J* = 15.0, 6.2 Hz, 2H), 2.46 (d, *J* = 15.0 Hz, 2H), 2.32 (s, 6H), 2.02 (t, *J* = 6.4 Hz, 2H), 1.41 (s, 6H), 1.03 (d, *J* = 6.7 Hz, 6H); ^{13}C NMR (101 MHz, $CDCl_3$) δ 144.7, 141.7, 141.6, 133.2, 132.9, 132.4, 120.7, 90.8, 85.7, 52.1, 41.8, 39.3, 20.6, 20.5, 16.9; mp = decomp > 155 °C *Trans* ^{1}H NMR (400 MHz, $CDCl_3$) δ 7.21 (s, 2H), 4.55 (s, 4H), 2.84 (app. p, 2H), 2.65 (dd, *J* = 14.6, 5.7 Hz, 2H), 2.39 (s, 6H), 2.27 (s, 6H), 2.24 (d, *J* = 14.7 Hz, 2H), 1.06 (d, *J* = 6.4 Hz, 6H); ^{13}C NMR (101 MHz, $CDCl_3$) δ 143.0, 142.1, 141.7, 133.6, 132.7, 131.1, 120.9, 90.7, 85.5, 52.1, 42.1, 39.4, 21.8, 19.5, 16.7. HRMS (APCI):: *m/z* calcd for $C_{30}H_{33}O_2$: 425.2475, found 425.2466 ($M+H^+$).

3-(5'-(3-(bis(4-methoxyphenyl)(phenyl)methoxy)prop-1-yn-1-yl)-2,2',4,4',7,7'-hexamethyl-2,2',3,3'-tetrahydro-[1,1'-biindenylidene]-5-yl)prop-2-yn-1-ol (2.10)

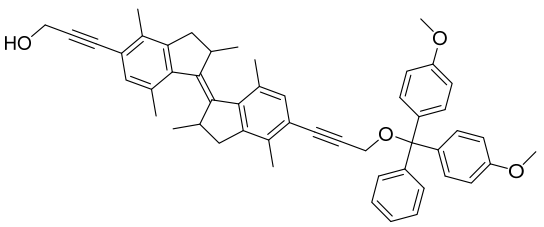

Motor *cis*-**2.3** (250 mg, 0.590 mmol) was dissolved in THF (4 mL) and cooled to 0 °C. Triethylamine (69 µL, 0.49 mmol) and dimethoxytrityl chloride (167 mg, 0.492 mmol) dissolved in THF (2 mL) were added and the reaction mixture was stirred overnight at room temperature. The reaction mixture was concentrated *in vacuo* under 30 °C. The crude product was purified on column chromatography (SiO_2, pentane/EtOAc/triethylamine (10:1:0.1 to 5:5:0.1). *Cis*-**2.10** was obtained as a white solid, in 36% yield (154 mg, 0.212 mmol). *Trans*-**2.10** was synthesized in

analogous manner. *Cis* ^{1}H NMR (400 MHz,CD_2Cl_2) δ 7.50 (d, *J* = 7.6 Hz, 2H), 7.38 (d, *J* = 8.9 Hz, 4H), 7.32 (t, *J* = 7.6 Hz, 2H), 7.23 (t, *J* = 7.3 Hz, 1H), 7.05 (s, 1H), 7.02 (s, 1H), 6.86 (d, *J* = 8.8 Hz, 4H), 4.51 (s, 2H), 4.01 (s, 2H), 3.78 (s, 6H), 3.36 (app. p, 2H), 3.09 (dd, *J* = 15.1, 6.4 Hz, 2H), 2.47 (d, *J* = 15.0 Hz, 2H), 2.34 (s, 6H), 1.55 (s, 6H), 1.05 (d, *J* = 6.7 Hz, 6H). *Trans* ^{1}H NMR (400 MHz, CD_2Cl_2) δ 7.52 (d, *J* = 7.5 Hz, 2H), 7.40 (d, *J* = 8.8 Hz, 4H), 7.33 (t, *J* = 7.6 Hz, 2H), 7.25 (t, *J* = 7.2 Hz, 1H), 7.20 (s, 1H), 7.18 (s, 1H), 6.87 (d, *J* = 8.8 Hz, 4H), 4.52 (s, 2H), 4.03 (s, 2H), 3.79 (s, 6H), 2.85 (app. p, 2H), 2.66 (dd, *J* = 14.7, 5.7 Hz, 2H), 2.41 (d, *J* = 1.8 Hz, 6H), 2.29 (m, *J* = 8.9 Hz, 8H), 1.07 (d, *J* = 6.4 Hz, 6H). HRMS (APCI): *m/z* calcd for $C_{51}H_{51}O_4$: 727.37819, found 727.37814 ($M+H^+$). Due to instability of the compound, no ^{13}C NMR spectra and melting points were measured.

3-(5'-(3-(bis(4-methoxyphenyl)(phenyl)methoxy)prop-1-yn-1-yl)-2,2',4,4',7,7'-hexamethyl-2,2',3,3'-tetrahydro-[1,1'-biindenylidene]-5-yl)prop-2-yn-1-yl (2-cyanoethyl) diisopropylphosphoramidite (2.11)

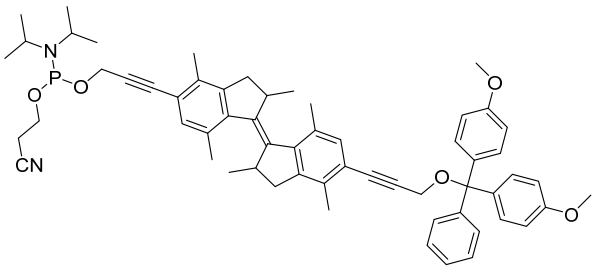

Cis-mono-DMT protected overcrowded alkene **2.10** (151 mg, 0.208 mmol) and DMAP (2.5 mg, 0.021 mmol) were dried overnight *in vacuo* in a 25 mL round bottom flask equipped with stirring bar. Anhydrous dichloromethane (4 mL) was added, followed by 2-cyanoethyl-*N*,*N*-diisopropylchlorophosphoramidite (69.7 µL, 0.312 mmol) and freshly distilled diisopropylethylamine (181 µL, 1.04 mmol). The reaction mixture was stirred at room temperature under an argon atmosphere. After 90 min, the crude reaction mixture was transferred straight onto a SiO_2 column and flushed through with DCM/hexane/trimethylamine 8:2:0.02. Phosphoramidite motor *cis*-**2.11** was obtained as a yellow solid. Due to instability of the compound, only limited characterization was performed before proceeding with the solid-phase synthesis. *Trans*-**2.11** could be obtained in analogous manner, but could not be separated from its major side product and was used as a mixture containing 80% of the dimer. *Cis*: ^{1}H NMR (400 MHz, CD_2Cl_2) δ 7.50 (d, *J* = 7.5 Hz, 2H), 7.39 (d, *J* = 8.9 Hz, 4H), 7.32 (t, *J* = 7.6 Hz, 2H), 7.24 (t, *J* = 7.3 Hz, 1H), 7.05 (s, 1H), 7.02 (s, 1H), 6.86 (d, *J* = 8.9 Hz, 4H), 4.59 (d, *J* = 4.5 Hz, 1H), 4.56 (d, *J* = 5.3 Hz, 1H), 3.95 – 3.82 (m, 2H), 3.78 (s, 6H), 3.66 (app. dp, 2H), 3.36 (app. p, 2H), 3.10 (dd, *J* = 15.1, 6.3 Hz, 2H), 2.66 (td, *J* = 6.4, 2.4 Hz, 2H), 2.48 (d, *J* = 15.0 Hz, 2H), 2.34 (2, 6H), 1.48 (s, 6H), 1.33 – 1.19 (m, 12H), 1.06 (d, *J* = 6.7 Hz, 6H).^{31}P NMR ($CDCl_3$) δ 147.1.

Trans: ^{31}P NMR (CD_2Cl_2) δ 147.0. ^{1}H NMR signals overlapping with side product.

2.11 References

1 J. D. Watson, F. H. C. Crick, *Nature* **1953**, *171*, 737–738.
2 M. R. Jones, N. C. Seeman, C. A. Mirkin, *Science* **2015**, *347*, 1260901.
3 H. Ledford, *Nature* **2016**, *531*, 156–159.
4 N. Goldman, P. Bertone, S. Chen, C. Dessimoz, E. M. LeProust, B. Sipos, E. Birney, *Nature* **2013**, *494*, 77–80.
5 S. Modi, M. G. Swetha, D. Goswami, G. D. Gupta, S. Mayor, Y. Krishnan, *Nat. Nanotechnol.* **2009**, *4*, 325–330.
6 H. Chen, H. Zhang, J. Pan, T.-G. Cha, S. Li, J. Andréasson, J. H. Choi, *ACS Nano* **2016**, *10*, 4989–4996.
7 F. Zhang, J. Nangreave, Y. Liu, H. Yan, *Nano Lett.* **2012**, *12*, 3290–3295.
8 S. M. Douglas, I. Bachelet, G. M. Church, *Science* **2012**, *335*, 831–834.
9 T. Gerling, K. F. Wagenbauer, A. M. Neuner, H. Dietz, *Science* **2015**, *347*, 1446–1452.
10 R. Weissleder, V. Ntziachristos, *Nat. Med.* **2003**, *9*, 123–128.
11 W. Szymański, J. M. Beierle, H. A. V. Kistemaker, W. A. Velema, B. L. Feringa, *Chem. Rev.* **2013**, *113*, 6114–6178.
12 A. S. Lubbe, W. Szymanski, B. L. Feringa, *Chem. Soc. Rev.* **2017**, *46*, 1052–1079.
13 P. C. Bevilacqua, J. M. Blose, *Annu. Rev. Phys. Chem.* **2008**, *59*, 79–103.
14 P. Svoboda, A. Di Cara, *Cell. Mol. Life Sci.* **2006**, *63*, 901–918.
15 Y. Yin, X. S. Zhao, *Acc. Chem. Res.* **2011**, *44*, 1172–1181.
16 R. L. Letsinger, T. Wu, *J. Am. Chem. Soc* **1994**, *116*, 811–812.
17 R. L. Letsinger, T. Wu, *J. Am. Chem. Soc.* **1995**, *117*, 7323–7328.
18 K. Yamana, A. Yoshikawa, H. Nakano, *Tetrahedron Lett.* **1996**, *37*, 637–640.
19 L. Wu, K. Koumoto, N. Sugimoto, *Chem. Commun.* **2009**, 1915–1917.
20 L. Wu, Y. Wu, H. Jin, L. Zhang, Y. He, X. Tang, *Med. Chem. Commun.* **2015**, *6*, 461–468.
21 N. Koumura, R. W. Zijlstra, R. A. van Delden, N. Harada, B. L. Feringa, *Nature* **1999**, *401*, 152–155.
22 M. M. Pollard, A. Meetsma, B. L. Feringa, *Org. Biomol. Chem.* **2008**, *6*, 507–512.
23 J. C. M. Kistemaker, *Autonomy and Chirality in Molecular Motors*, PhD thesis, University of Groningen 2017.
24 T. M. Neubauer, T. van Leeuwen, D. Zhao, A. S. Lubbe, J. C. M. Kistemaker, B. L. Feringa, *Org. Lett.* **2014**, *16*, 4220–4223.
25 M. Safak, F. E. Alemdaroglu, Y. Li, E. Ergen, A. Herrmann, *Adv. Mater.* **2007**, *19*, 1499–1505.
26 K. Yamana, A. Yoshikawa, R. Noda, H. Nakano, *Nucleos. Nucleot.* **1998**, *17*, 233–242.
27 K. Yamana, K. Kan, H. Nakano, *Bioorg. Med. Chem.* **1999**, *7*, 2977–2983.
28 F. D. Lewis, Y. Wu, X. Liu, *J. Am. Chem. Soc.* **2002**, *124*, 12165–12173.
29 V. P. Antao, S. Y. Lai, I. Tinoco Jr., *Nucleic Acids Res.* **1991**, *19*, 5901–5905.
30 F. D. Lewis, X. Liu, Y. Wu, S. E. Miller, M. R. Wasielewski, R. L. Letsinger, R. Sanishvili, A. Joachimiak, V. Tereshko, M. Egli, *J. Am. Chem. Soc.* **1999**, *121*, 9905–9906.
31 J. Wang, L. Hou, W. R. Browne, B. L. Feringa, *J. Am. Chem. Soc.* **2011**, *133*, 8162–8164.
32 D. Zhao, T. M. Neubauer, B. L. Feringa, *Nat. Commun.* **2015**, *6*, 6652.